TECHNICAL NOTE • OPEN ACCESS

A system to test 2D optoelectronic devices in high vacuum

To cite this article: Qinghua Zhao *et al* 2020 *J. Phys. Mater.* **3** 036001

View the article online for updates and enhancements.

Journal of Physics: Materials

TECHNICAL NOTE

A system to test 2D optoelectronic devices in high vacuum

Qinghua Zhao[1,2,3], Felix Carrascoso[3], Patricia Gant[3], Tao Wang[1,2], Riccardo Frisenda[3] and
Andres Castellanos-Gomez[3]

1   State Key Laboratory of Solidification Processing, Northwestern Polytechnical University, Xi'an, People's Republic of China
2   Key Laboratory of Radiation Detection Materials and Devices, Ministry of Industry and Information Technology, Xi'an, People's
    Republic of China
3   Materials Science Factory, Instituto de Ciencia de Materiales de Madrid (ICMM-CSIC), Madrid, Spain

E-mail: riccardo.frisenda@csic.es and andres.castellanos@csic.es

Abstract

The exploration of electronic and optoelectronic properties of two-dimensional (2D) materials has become one of the most attractive line of research since the isolation of graphene. Such '*all-surface materials*' present a strong sensitivity to environmental conditions and thus characterization of the devices based on these materials usually requires measurement systems operating in high-vacuum. However, conventional optoelectronic probe-station testing systems are are not compatible with high vacuum operation and vacuum-compatible versions are rather expensive. Here, we present a high vacuum system specifically designed to test electronic and optoelectronic devices based on 2D materials. This system can be implemented with low budget and it is mostly based on the assembly of commercially available standard vacuum and optic components. Despite the simplicity of this system we demonstrate full capabilities to characterize optoelectronic devices in a broad range of wavelengths with fast pumping/venting speed and possibility of modulating the device temperature (room temperature to $\sim$150 $^\circ$C).

1. Introduction

Since the isolation of graphene and other 2D materials [1–3], the scientific community has worked to apply these nanomaterials in several electronic and optoelectronic devices [4, 5]. Being '*all-surface materials*', the properties of 2D materials are highly sensitive to the environmental conditions [6–11]. This has made it necessary the use of experimental testing systems that allow for a control of the atmospheric condition [12, 13]. In many cases, high vacuum is needed to get rid of the adsorbed moisture layer at the surface [10]. Conventional optoelectronic testing tools such as probe stations are not compatible with high vacuum operation and vacuum-compatible versions are rather expensive.

In this work we present a compact and inexpensive high vacuum system to characterize electronic and optoelectronic devices based on 2D materials. The system is mainly based on the assembly of standard high vacuum elements, requiring only few home-built parts. We supplement the system with probes that facilitate the electrical connection to the devices, and we employ fiber optic-based illumination to study the optoelectronic properties of the devices. We show that the system can be evacuated quickly to reach low pressure conditions and that a fast control of the device temperature can be realized. We illustrate the operation of the system by characterizing the performance of Au–InSe–Au devices in dark and under external controlled illumination in high vacuum conditions.

Tables 1–3 summarize the commercially available components, indicating distributor and part-number, necessary for the assembly of the devices. Figure 1(a) shows a scheme of the high vacuum parts (with model information) needed to assemble the vacuum chamber and 1b shows the actual photograph of the assembled setup fixed on a manual X–Y placement platform with a travel range of 30 mm × 30 mm and an adjustment accuracy of 1 μm. Two KFA25/50A reducers at the bottom of the chamber are used for the connection of molecular turbo pumping station (indicated as 'air out' in the schematics) and venting valve ('air in'), which

Table 1. Summary of the components needed for the assembly of the small vacuum chamber. Links provided in the digital version of the manuscript.

| Vendor	Quantity	Part number	Description	Unit price
	1	ISO100/50A	ISO-K 100 to NW50KF adaptor	97.00
	2	ISO100AV	ISO-K 100 centering ring	16.50
	12	ISO63CA	ISO-K 100 clamps	1.90
	1	KX5/50/50	NW50KF 5-way cross	240.00
	5	KF50/RA	NW50KF centering ring	5.00
Hositrad	5	KF50/C	NW50KF clamps	6.00
	2	KFA25/50A	NW25KF to NW50KF (reducer)	18.00
	2	KF50/BA	NW50KF blanks	6.00
	1	HVP-ISO100	NW100 ISO-K viewport	195.00
	1	KF25/RA	NW25KF centering ring	2.25
	1	KF25/C	NW25KF clamps	2.50
USA lab	1	KF25PRV	KF25 Venting Valve	59.00
Lesker	1	ISO100-K (5.12" OD)	Full Nipple, Clamp Style	138.70
RS	7	295-7942	Hermetic BNC connector	7.97
Optics-Focus	1	MAXY-125L-25	XY placement platform	180.00
Linkam	3	—	Magnetic probe-tip holder	280
			Total:	1967.78 €

Table 2. Summary of the components needed for the assembly of the optical system used for inspection/illumination of the devices. Links provided in the digital version of the manuscript.

| Vendor	Quantity	Part number	Description	Unit price
AMScope	1	SKU: SA-HG-2	Solid Aluminum Single-arm Boom Stand	202.99
Aliexpress	1	ZOOM_LENS	400x zoom lens with coaxial illuminator	185.99
	1	DIGI_CAM	21 MPix HDMI + USB camera	77.88
	1	M530F2	High-power fiber coupled LED source ($\lambda = 530$ nm, other wavelengths available)	371.82
	1	LEDD1B	LED driver	294.11
	1	M28L01	Multimode optical fiber (core 400 μm, other core sizes available)	84.59
Thorlabs	1	SCP05	Miniature XY translator stage for the optical fiber (see Figure 5b3)	146.49
	1	SM05SMA	Adapter from optical fiber to miniature XY stage (see Figure 5b3)	27.54
			Total:	1391.41 €

Table 3. Summary of the auxiliary equipment used here to pump down the chamber and to perform the electrical measurements.

| Vendor	Quantity	Model	Description	Unit price
Keithley	1	Keithley 2450	Source measurement unit for the electrical measurements of devices	5250.00
Edwards	1	T-Station 85H Dry NW40	Turbo pump station with wide range pressure gauge	6700.00
			Total:	11 950.00 €

allows fast chamber atmosphere switching between vacuum and air. Figure 1(c) shows the interior of the chamber after removing the cap. A machined cylinder piece (marked by squared gray dash line in figure 1(c)) is placed inside the chamber in order to reduce the pumping volume and to place the sample closer to the system optical window. Although a smaller chamber size would have led to even faster pumping speed, we choose to base our design in an ISO-100 standard size in order to facilitate the sample and probe placement operations. In the last years we have tested smaller chamber sizes finding them quite uncomfortable for the operator. The electrical feedthrough (homebuilt, see more details below) allows connecting the electronic components to perform the electrical measurements: source measure unit for electrical characterization of devices, programmable benchtop power supply to control the heater mounted on sample stage and multi-meter to test the thermistor resistance.
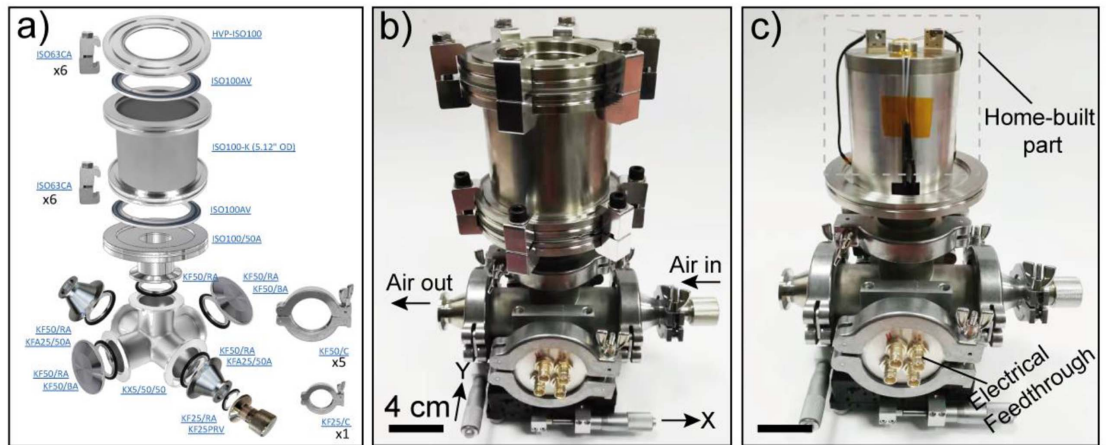
Figure 1. (a) Scheme of the commercial high-vacuum parts used for vacuum chamber building. (b), (c) Photographs with (b) and without (c) the cap of the assembled vacuum chamber mounted onto a XY stage. The home-built parts are highlighted in panel (c).
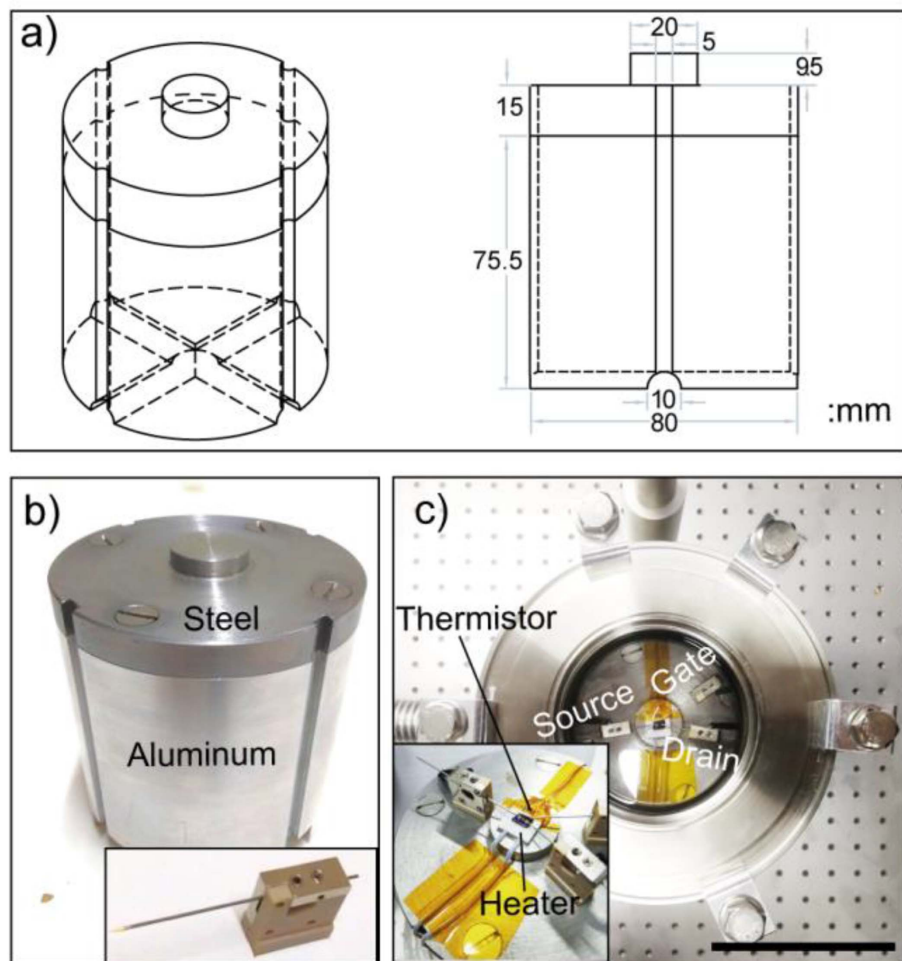
Figure 2. Home-built sample stage. (a) Isometric 3D sketch of home-built sample stage (left panel) and side view with indicated the corresponding dimensions in millimeters (right panel). (b) Close-up photographs of the as-machined home-built sample stage and the miniature probe with bottom magnets. (c) Top view of the sample stage surface as seen through the optical window. The inset is a close-up image of the ceramic heater, thermistor and three miniature probes (source, drain and gate). The scale bar is 50 mm.
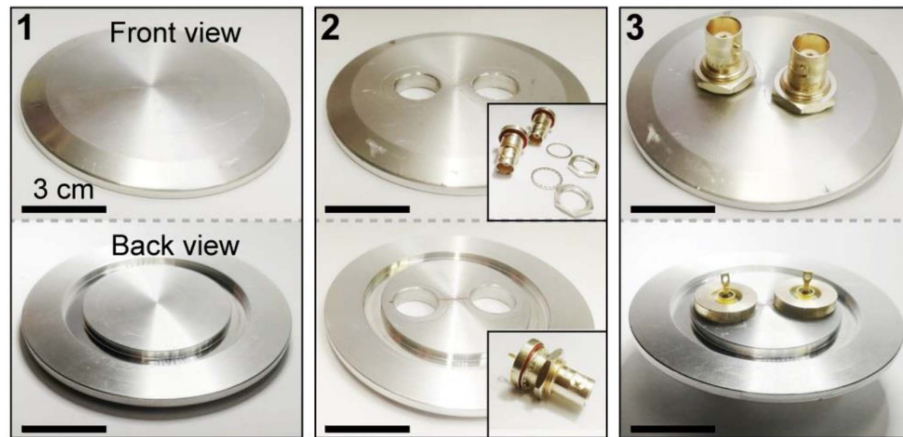
**Figure 3.** Fabrication process of an electrical feedthrough. The front view and back view of a KF50 flange (1), the KF50 flange with two drilled holes (2) and two hermetic BNC nut-jam connectors are screwed on the KF50 flange (3).
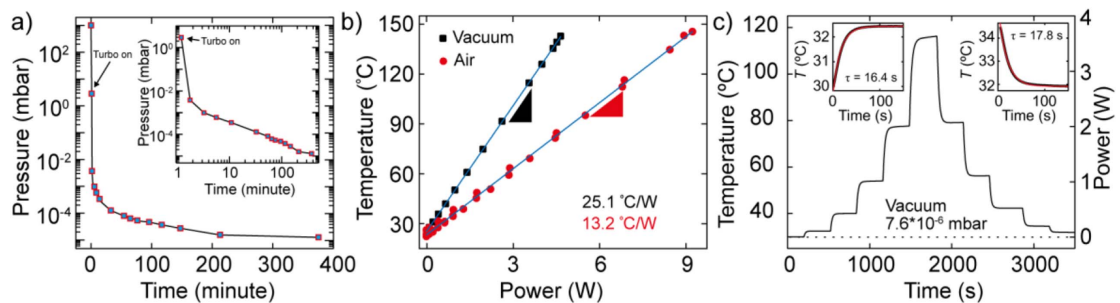
Figure 4. Pressure and temperature calibration of the vacuum chamber. (a) Recorded pressure in the chamber as a function of molecular turbo pumping time. The inset is the plot of pressure versus time in log-log scale. (b) Relationship between surface temperature and working power of heater measured under atmosphere and vacuum ($\sim 10^{-5}$ mbar) condition. (c) Continuous temperature control recorded in time as a function of working power of heater under high-vacuum (7.6×10^{-6} mbar) condition. The insets are exponential growth/decay fits of the heating (left) and cooling (right) temperature as a function of time.

The details of home-built parts necessary to complete the vacuum chamber system are shown in figures 2 and 3, respectively. Figure 2(a) shows a sketch of the home-built sample stage that sits inside the vacuum chamber. The corresponding dimensions are marked in the left panel of figure 2(a). Figure 2(b) shows a close-up picture of the home-built sample stage cylinder which consists of the top (magnetic) steel part and the bottom supporting aluminum cylinder part. The top steel part surface has been supplemented with a ceramic heater plate to heat up the devices (up to 200 °C), a thermistor used for temperature sensing (note that the thermistor used here limits the maximum operation temperature to 150 °C). Three miniature probes (Linkam) attached with magnets are used to contact the electrical pads of the devices to establish the source, drain and gate connections. The heater, the thermistor and the three probes are connected to a home-built BNC electrical feedthrough through coaxial cable (RG 178, BELDEN). An example of such an electrical feedthrough fabrication process is shown in figure 3. Briefly, two holes are drilled on a blank KF50 flange and hermetic BNC nut-jam connectors are screwed to ensure a vacuum tight sealing.

Figure 4(a) shows the internal pressure of the chamber as a function of time when connected to a molecular turbo pumping station (Edwards, T-station 85H). Due to the reduced pumping volume the chamber reaches low enough pressure in relatively short period of time. The internal pressure of chamber can be reduced from atmospheric pressure to $\sim 10^{-4}$ mbar within less than ~ 30 min of pumping time. Note that upon pumping over longer periods of time (typically 10 h overnight) we have regularly achieved pressures lower than 10^{-5} mbar. Figure 4(b) shows the calibration of the ceramic heater, the temperature values are recorded from room temperature up to ~ 150 °C in ambient (red circles) and in vacuum (black squares) conditions by controlling the heater working power. The good agreement between the experimental data and the linear fit (blue line) confirm that the heater temperature depends linearly on the heater working power. From the linear fits we find the heater calibration values 13.2 °C W^{-1} in air and 25.1 °C W^{-1} in vacuum. To test the temperature response time of the system we recorded the temperature as a function of time while the heater working power is changed in increasingly large steps, from 0 W to 4 W, every 600 s.
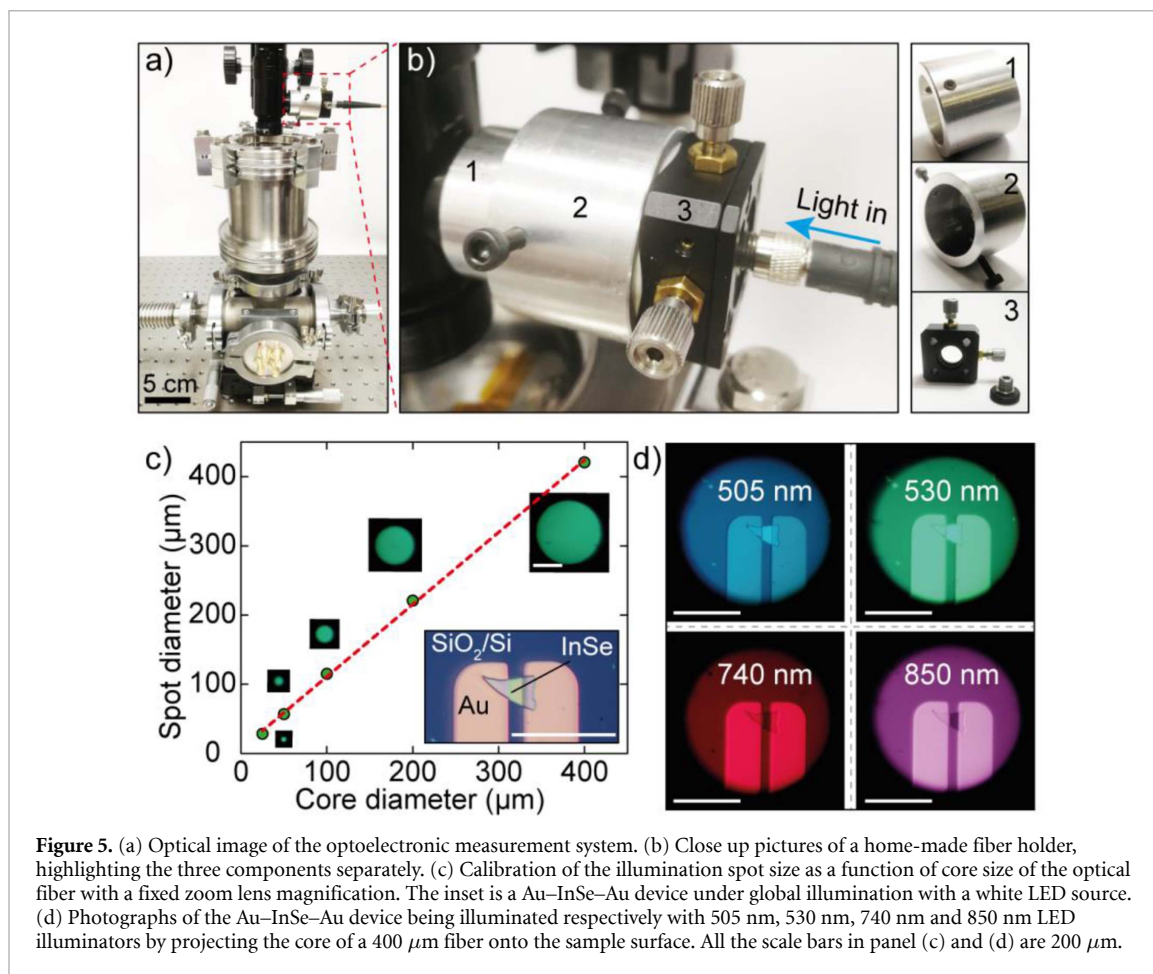
Figure 5. (a) Optical image of the optoelectronic measurement system. (b) Close up pictures of a home-made fiber holder, highlighting the three components separately. (c) Calibration of the illumination spot size as a function of core size of the optical fiber with a fixed zoom lens magnification. The inset is a Au–InSe–Au device under global illumination with a white LED source. (d) Photographs of the Au–InSe–Au device being illuminated respectively with 505 nm, 530 nm, 740 nm and 850 nm LED illuminators by projecting the core of a 400 μm fiber onto the sample surface. All the scale bars in panel (c) and (d) are 200 μm.

From figure 4(c), one can observe that after turning up or down the heater power a fast temperature raise or drop is followed by a stable temperature level. Details on the heating and cooling temperature change are shown in left and right inset panel in figure 4(c). Both of the processes are well fitted to a exponential growth/decay function with the time parameters $\tau \approx$ 16.4–17.8 s.

In order to study the optoelectronic response of devices we place the vacuum chamber under a long working distance zoom lens that allows one both imaging the devices and shining light on them. Figure 5(a) shows an optical image after mounting the chamber under the zoom lens imaging/illumination system. In order to photo-excite the devices with a controlled illumination, the coaxial zoom lens system can be supplemented with a home-built part (highlighted with a red dashed square in figure 5(a)) that holds a multimode optical fiber. The details about the home-made fiber holder are shown by a close-up picture in figure 5(b) and the fabrication details can be found in figure S1 stacks.iop.org/JPhysMaterials/3/036001/mmedia. The three isolated components are shown in the right panels. The fiber holder allows one to place the fiber core on the image plane of the zoom lens system, thus projecting an image of the fiber core on the sample that produces a circular spot with uniform power density on the sample surface. Note that the size of the circular spot is both controlled by the optical fiber core size and the magnification of the zoom lens system. Figure 5(c) shows a comparison of the spots acquired by connecting 5 optical fibers with different core sizes ranging from 25 μm to 400 μm. A linear relationship between the projected illumination spot size (on a 285 nm SiO$_2$/Si substrate) and the optical fiber core diameter (for a fixed magnification of the zoom lens) is obtained. The projection of the fiber core on the sample in combination with high-power fiber coupled LED sources (Thorlabs) yields highly homogenous and speckle-free spots that result very convenient to determine the figures-of-merit of a photodetector device, like photoresponsivity and detectivity. We address the reader to the supporting information (figure S2) for a comparison between the intensity profile obtained with this illumination method with respect to a Gaussian-shape laser spot. Moreover, this illumination method allows for easily change of the illumination wavelength without a substantial change in the spot size and shape. Figure 5(d) shows a Au–InSe–Au device illuminated by projecting the core of a 400 μm fiber coupled LED illuminators with 505–850 nm of central wavelength.

In the following, we illustrate the operation of the system by characterizing the optoelectronic properties of the Au–InSe–Au photodetector (shown in the inset in figure 5(c)), assembled by deterministic placement
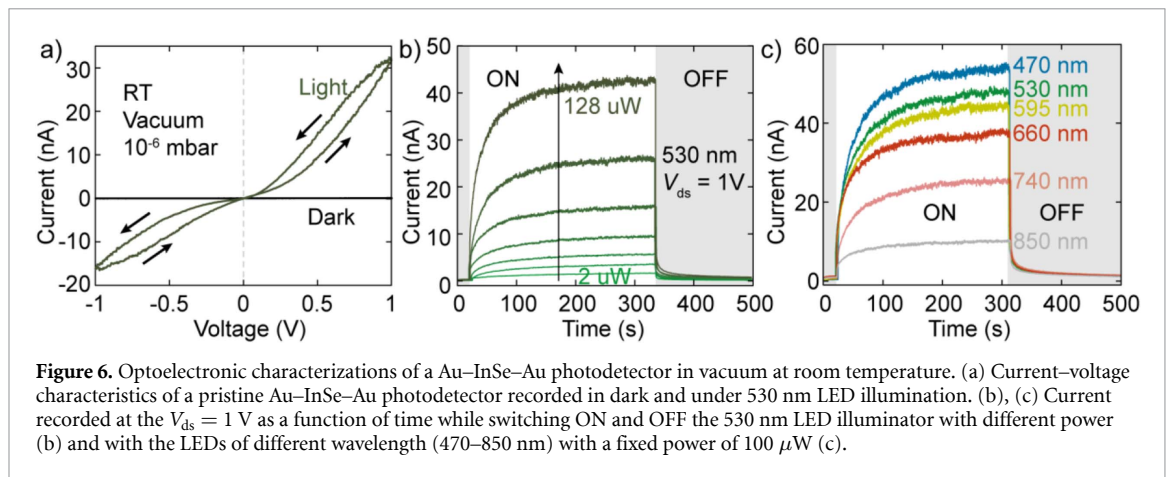
Figure 6. Optoelectronic characterizations of a Au–InSe–Au photodetector in vacuum at room temperature. (a) Current–voltage characteristics of a pristine Au–InSe–Au photodetector recorded in dark and under 530 nm LED illumination. (b), (c) Current recorded at the $V_{ds} = 1$ V as a function of time while switching ON and OFF the 530 nm LED illuminator with different power (b) and with the LEDs of different wavelength (470–850 nm) with a fixed power of 100 μW (c).
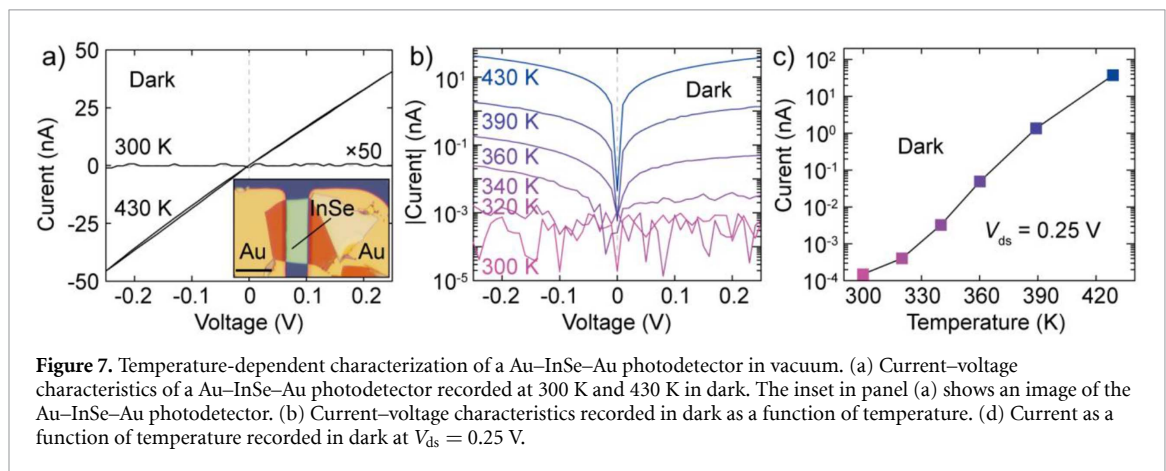
Figure 7. Temperature-dependent characterization of a Au–InSe–Au photodetector in vacuum. (a) Current–voltage characteristics of a Au–InSe–Au photodetector recorded at 300 K and 430 K in dark. The inset in panel (a) shows an image of the Au–InSe–Au photodetector. (b) Current–voltage characteristics recorded in dark as a function of temperature. (d) Current as a function of temperature recorded in dark at $V_{ds} = 0.25$ V.

of an InSe flake onto pre-patterned gold electrodes [14–16], under high vacuum condition at room temperature. We use a source measurement unit (Keithley 2450) to perform electrical measurements on the device in the dark state and upon illumination. Current–voltage (*I*–*V*) and current–time (*I*–*t*) curves are typical characteristics for measuring optoelectronic properties of photodetectors. Figure 6(a) shows the source-drain current as a function of voltage of a pristine Au–InSe–Au photodetector recorded under dark condition and illumination of 530 nm LED illuminator. Negligible current flows through the device when kept in dark condition, while an obvious increase in current can be observed when the device was measured under illumination due to the photogeneration of charge carriers in the device [17]. The current hysteresis observed in the light current–voltage curve suggests the existence of traps in pristine InSe crystals under vacuum condition [8]. The response of the device to light is then studied by measuring the source-drain current flowing through the device at the fixed bias voltage as a function of time while the illumination is switched ON and OFF. Figure 6(b) shows an example of that kind of measurement that allows determining both the photocurrent (the difference between the current with light ON and light OFF) and the response time of the device. The response time of a photodetector is usually determined by measuring the time that it takes to go from the 10% to the 90% (or from the 90% to the 10%) of the generated photocurrent under modulated excitation illumination, either in the rising or falling edge [17]. By repeating the measurements for different illumination wavelength at same power one can obtain the photocurrent spectrum of the device.

In order to demonstrate the temperature control of the setup, we carry out a set of optoelectronic characterization of an Au–InSe–Au device by varying the testing temperature. Figure 7(a) shows a linear plot of current–voltage characteristics of the Au–InSe–Au photodetector plotted recorded at 300 K and 430 K in dark condition. Noise-level current flows through the device in dark at 300 K while the current increases noticeably when the temperature is increased to 430 K. The temperature dependency of the *I*–*V* curves of the device recorded in dark with semi-logarithmic scale are reported in figure 7(b). The *I*–*V*s recorded while increasing the temperature from *T* = 300 K to *T* = 430 K show a current increase both at positive and negative bias voltages and an increase of the symmetry. Based on the *I*–*V*s recorded in dark, we extract the current value at $V_{ds} = 0.25$ V and plot them as a function of temperature in figure 7(c). The dark current flowing through the device increases with the temperature in an exponential way (that appears linear in the

semi-logarithmic representation of figure 7(c)), this could be due to an increase of carrier density by thermal excitation in the InSe or to a lowering of the contact resistance [18–20].

2. Conclusions

In summary, we presented an inexpensive system to characterize optoelectronic devices based on 2D materials in high-vacuum. The whole system can be assembled using commercially available standard vacuum elements and only few home-built parts are needed. We demonstrate that this system can reach a pressure $<10^{-5}$ mbar and it allows for a fast testing of temperature dependence, from room temperature to $\sim150\,^{\circ}$C. We show how the system can be used to characterize devices based on 2D materials. In fact, we illustrate the operation of our system by testing the electrical and optoelectronic characteristics of a InSe device at a pressure of 10^{-6} mbar with different illumination powers (ranging from 2 μW to 128 μW), with different wavelengths (from 470 nm to 850 nm) and at different temperatures (room temperature to 130 $^{\circ}$C). This setup can be an alternative to more expensive commercially available systems and thus we believe that such kind of system can be easily implemented in labs with low budget and satisfy the characterization requirements for 2D materials optoelectronic devices.

ORCID iDs

Riccardo Frisenda ⬤ https://orcid.org/0000-0003-1728-7354
Andres Castellanos-Gomez ⬤ https://orcid.org/0000-0002-3384-3405

References

[1] Novoselov K S, Geim A K, Morozov S V, Jiang D, Zhang Y, Dubonos S V, Grigorieva I V and Firsov A A 2004 *Science* **306** 666–9
[2] Novoselov K, Mishchenko A, Carvalho A and Neto A C 2016 *Science* **353** aac9439
[3] Backes C, Abdelkader A M, Alonso C, Andrieux-Ledier A, Arenal R, Azpeitia J, Balakrishnan N, Banszerus L, Barjon J and Bartali R 2020 *2D Mater.* **7** 022001
[4] Wang Q H, Kalantar-Zadeh K, Kis A, Coleman J N and Strano M S 2012 *Nat. Nanotechnol.* **7** 699–712
[5] Bonaccorso F, Sun Z, Hasan T and Ferrari A 2010 *Nat. Photon.* **4** 611
[6] Yang S, Jiang C and Wei S-H 2017 *Appl. Phys. Rev.* **4** 021304
[7] Wang G, Pandey R and Karna S P 2017 *Wiley Interdiscip. Rev. Comput. Mol. Sci.* **7** 1
[8] Zhao Q, Wang W, Carrascoso-Plana F, Jie W, Wang T, Castellanos-Gomez A and Frisenda R 2019 *Mater. Horiz.* **7** 252–62
[9] Zhao Q, Frisenda R, Gant P, Perez de Lara D, Munuera C, Garcia-Hernandez M, Niu Y, Wang T, Jie W and Castellanos-Gomez A 2018 *Adv. Funct. Mater.* **28** 1805304
[10] Island J O, Steele G A, van der Zant H S and Castellanos-Gomez A 2015 *2D Mater.* **2** 011002
[11] Gant P, Carrascoso F, Zhao Q, Ryu Y K, Seitz M, Prins F, Frisenda R and Castellanos-Gomez A 2020 *2D Mater.* **7** 025034
[12] Qiu H, Xu T, Wang Z, Ren W, Nan H, Ni Z, Chen Q, Yuan S, Miao F and Song F 2013 *Nat. Commun.* **4** 2642
[13] Park W, Park J, Jang J, Lee H, Jeong H, Cho K, Hong S and Lee T 2013 *Nanotechnology* **24** 095202
[14] Castellanos-Gomez A, Buscema M, Molenaar R, Singh V, Janssen L, Van der Zant H S and Steele G A 2014 *2D Mater.* **1** 011002
[15] Zhao Q, Wang T, Ryu Y K, Frisenda R and Castellanos-Gomez A 2020 *J. Phys. Mater.* **3** 016001
[16] Frisenda R, Navarro-Moratalla E, Gant P, De Lara D P, Jarillo-Herrero P, Gorbachev R V and Castellanos-Gomez A 2018 *Chem. Soc. Rev.* **47** 53–68
[17] Buscema M, Island J O, Groenendijk D J, Blanter S I, Steele G A, van der Zant H S and Castellanos-Gomez A 2015 *Chem. Soc. Rev.* **44** 3691–718
[18] Nouchi R 2014 *J. Appl. Phys.* **116** 184505
[19] Rhoderick E H 1982 *IEE Proc. I Solid State Electron Devices* **129** 1
[20] Sze S M and Ng K K 2006 *Physics of Semiconductor Devices* (New York: Wiley)